Lawrence Berkeley National Laboratory

Title
Fundamental limits of positron emission mammography

Permalink
https://escholarship.org/uc/item/6t79c7q6

Authors
Moses, William W.
Qi, Jinyi

Publication Date
2001-06-01

Peer reviewed

Fundamental Limits of Positron Emission Mammography*

William W. Moses and Jinyi Qi

Lawrence Berkeley National Laboratory, University of California, Berkeley, CA 94720 USA

Abstract

We explore the causes of performance limitation in positron emission mammography cameras. We compare two basic camera geometries containing the same volume of 511 keV photon detectors, one with a parallel plane geometry and another with a rectangular geometry. We find that both geometries have similar performance for the phantom imaged (in Monte Carlo simulation), even though the solid angle coverage of the rectangular camera is about 50% higher than the parallel plane camera. The reconstruction algorithm used significantly affects the resulting image; iterative methods significantly outperform the commonly used focal plane tomography. Finally, the characteristics of the tumor itself, specifically the absolute amount of radiotracer taken up by the tumor, will significantly affect the imaging performance.

I. INTRODUCTION

The past several years have seen a number of designs for PET cameras optimized to image the breast [1-9], commonly known as Positron Emission Mammography or PEM cameras. The guiding principal behind PEM instrumentation is that a camera whose field of view is restricted to a single breast will have significantly higher performance and lower cost than a conventional PET camera. Performance improvements are expected in two areas: solid angle coverage and attenuation. By placing the detectors close to the breast, the PEM geometry is able to subtend more solid angle around the breast than a conventional PET camera. In addition, gamma rays emitted in the breast have to pass through at most one attenuation length (~10 cm) of tissue in the PEM geometry, but may have to travel through as much as four attenuation lengths of tissue in a conventional PET camera. These two factors significantly increase the sensitivity (the detected coincident event rate per unit activity in the field of view) in the PEM geometry.

The field of "conventional" PET is mature enough that the general design tradeoffs are well understood [10, 11] and there are few major differences between the fundamental parameters of different PET cameras (such as detector ring and patient port diameters, axial extent, gamma ray detector performance, and methods for image reconstruction and attenuation correction). While many of the same principles hold true for PEM, PEM has some unique features that require different tradeoffs to be made. The purpose of this paper is to explore some of the PEM camera design aspects that fundamentally limit their performance, concentrating on those aspects that are significantly different than conventional PET.

II. CAMERA DESIGN

In order to quantify the effects of the design tradeoffs, it is useful to define a "standard" design to use as a quantitatively
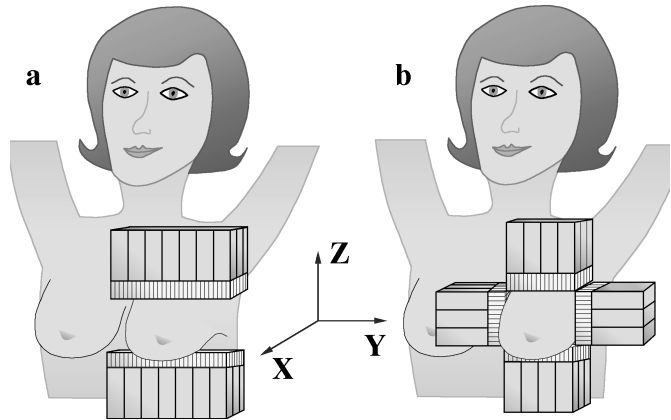
Figure 1. The two PEM camera geometries simulated in this paper. The parallel plane geometry is shown in a), the rectangular geometry in b).

reference. There is, however, no consensus among PEM camera designers on the "correct" geometry, and the sizes of many of the cameras that have been implemented have been heavily influenced by the properties of the available components rather than by pure performance optimization. Lacking a consensus, we choose as a "standard" PEM camera the geometry shown in Figure 1a. It consists of two parallel planes of detectors, each plane being 17.5 cm wide and 7.5 cm deep, with a spacing of 7.5 cm between planes. The detectors are assumed to have 3 mm spatial resolution, to be 30 mm deep, and to be made of LSO scintillator material [12] which has an attenuation length for 511 keV photons of 1.2 cm. All valid time coincidences between any detector element in one plane and any detector element in the other plane are kept. The orientation of the coordinate axes is also shown in Figure 1, with the origin located at the center of the field of view.

Throughout the paper, this parallel plane geometry is compared to the rectangular geometry shown in Figure 1b. Conceptually, this rectangular geometry would result if a 7.5 cm section of each plane in the parallel plane camera were detached, rotated 90°, and placed to cover the gap between planes. The field of view of the rectangular camera is 10 cm wide, 7.5 cm deep, and 7.5 cm high. As before, valid time coincidences between any detector element in one plane and any detector element in any of the other three planes is kept. This rectangular camera has the same volume, number, and type of detector elements as the planar camera, and so the cost should be similar. In addition, it has the same field of view as the planar camera, provided that the field of view of the planar camera is restricted to its central 10 cm in the y-direction.

Both these designs assume detectors that are capable of measuring the interaction depth within the scintillator crystal. Ability to measure this interaction depth is crucial for PEM cameras, where the object to be imaged is in close proximity to the detectors. As Figure 2 shows, many gamma rays will penetrate a significant distance into the detectors before they
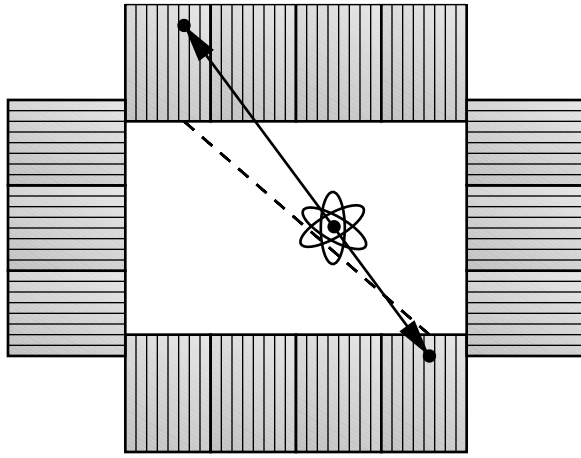
Figure 2. If the interaction position of gamma rays that penetrate into the detector module is assigned to the front face of the detector element, mis-positioning errors occur as the line connecting these points does not go through the source (the dotted line). If the interaction depth in the detector is measured, then the position is no longer assigned to the front face and the mis-positioning error is eliminated (solid line).

interact and are detected. If the interaction depth within a detector element is not measured (as is the case with virtually all conventional PET detector modules), then the interaction position is assigned to the front face of the detector element that the interaction occurs in. A line joining the two such assigned points may not pass through the actual source position, resulting in mis-positioning errors and degradation of the spatial resolution. If the interaction depth is measured, the line joining the two measured interaction positions will pass through the actual source position and no mis-positioning errors will result. The camera designs evaluated in this paper assume that the 30 mm depth of the scintillator crystal is divided into eight sections in depth (each 3.75 mm deep), and that the detector is able to properly identify the section that an interaction occurs in.

III. GEOMETRIC ACCEPTANCE

Figure 3 compares the geometric acceptance for a point source placed in the central horizontal (z=0) plane of the two PEM camera designs. The geometric acceptance at any point is defined as the fraction of the 4π solid angle surrounding a source placed at that point in which both back-to-back emanations from the source impinge on regions covered by the detector. This does not include the affect of attenuation of the gamma rays before they reach the detectors or detector efficiency. The overall features for the two geometries are similar – there is a significant decrease in solid angle coverage
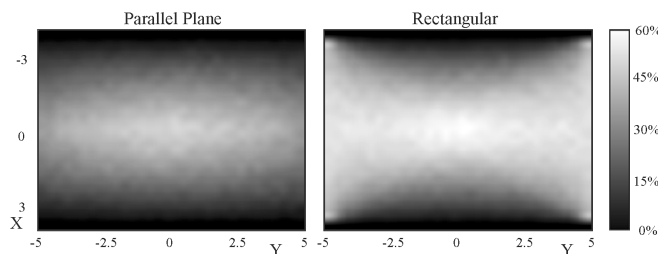
Figure 3. Solid angle coverage versus position for a point source placed on the central horizontal (z=0) plane of the planar and rectangular PEM cameras. Units are cm.

as the source nears the front or back of the camera (large absolute value of x) due to the "holes" (detector-free regions near the chest wall and nipples) in the cameras, but the solid angle coverage varies only weakly as one moves side to side (*i.e.* in the y-direction). There are some differences however; the rectangular camera shows less variation as a function of y-value and also has higher solid angle coverage, with a maximum of 60% of 4π as opposed to 45% of 4π with the parallel plane geometry. This compares with approximately 2% of 4π for conventional PET. If attenuation effects are included, then the mean acceptance for a 7.5 cm x 7.5 x cm x 10 cm uniform source distribution is 6% for the parallel plane geometry and 14% for the rectangular geometry.

IV. ANGULAR COVERAGE

The raw data from the PEM camera is converted into a volumetric image of the radiotracer distribution using computed tomography [13], which is the mathematical technique of reconstructing an *n*-dimensional object from (*n-1*)-dimensional projections of the object taken at many angles. In conventional PET, the three dimensional images are usually formed by stacking together two dimensional images, with each image being formed from multiple one dimensional projections. Fourier-based methods are often used to do this, and these methods generally require that the projections are taken at approximately 100 angles that evenly span the angular range from 0 to π (coverage to 2π is redundant, as the projection at angle $\theta+\pi$ is identical to the projection at angle θ).

Figure 4 shows that the parallel plane system has a large gap in the angular coverage in directions that are nearly parallel to the y-axis. These projections, if present, would constrain the extent of a point source in the z-direction. While there are reconstruction techniques that can operate with incomplete angular coverage, they are hampered by the loss of information at these angles and so are likely to have degraded spatial resolution in the z-direction. Thus, we expect that images from the parallel plane camera will suffer from some blurring or degraded spatial resolution in the z-direction, and further expect that this degradation will be absent in images from the
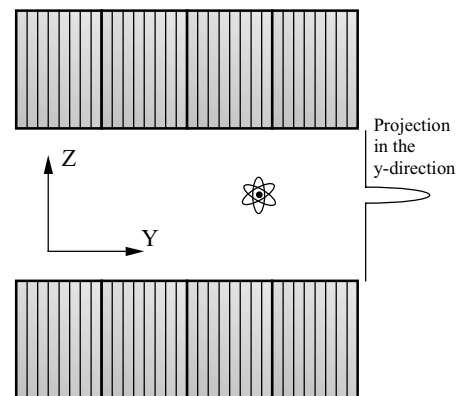
Figure 4. Gamma rays that emanate from the source in directions near the y-axis are not detected in the planar geometry, therefore the projections of the source near the y-axis are not measured. These projections are measured with the rectangular geometry.
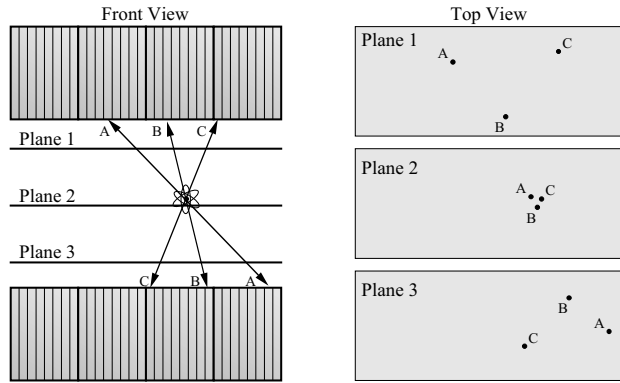
Figure 5. In focal plane tomography, lines are drawn between the interaction points of coincident events in the camera (such as lines AA, BB, and CC at the left). The intersection point of these lines with multiple imaging planes (Planes 1–3) is computed and the pixel value at these points are incremented, as shown on the right (points A, B, and C in each of the three planes). The image will be "in-focus" on planes that intersect the source, and progressively "out-of-focus" for planes at increasing distance from the source.

rectangular camera, as it is able to acquire projection data at these angles.

V. RECONSTRUCTION ALGORITHMS

Because of these large gaps in the angular coverage, most parallel plane PEM cameras do not use the reconstruction techniques that are standard for conventional PET cameras (such as Fourier-based filtered backprojection), but instead use a technique known as focal plane tomography [14]. With this technique, several imaginary imaging planes are placed in the field of view. Whenever a pair of coincident 511 keV gamma rays are detected, a line is drawn connecting the interaction points and the point of intersection of this line with each of the imaging planes is computed. The intensity at this point on the imaging plane (*i.e.* the pixel value of the image) is then increased, usually by an amount proportional to the inverse of the detection efficiency for a point source placed at this location [15]. Figure 5 shows that a point source placed close to an imaging plane will yield an excellent image in that plane (where it is "in focus"), but will yield much poorer images in imaging planes that are farther away (where it is "out of focus"). The advantages of this method are that it is simple to implement and very rapid to compute (real-time reconstruction is possible). The main disadvantage is that the algorithm places activity in *every* plane, even though the event originated in (or near) a single plane. Even though this mis-placed activity many be diffuse, it builds up rapidly when distributed sources are imaged, forming a broad background that significantly reduces image contrast.

The same raw data sets used by the focal plane tomography algorithm can also be reconstructed using iterative reconstruction algorithms similar to those used in "conventional" PET [16, 17]. The general concept behind such algorithms is relatively simple: an estimate of the 3-dimensional activity distribution is assumed, a mathematical model of the camera response is used to simulate the pattern of coincident event detections that the camera would observe with

this activity distribution, and the pattern of "detected" events derived from the estimated activity distribution is compared to the measured pattern of events. The differences are noted, used to revise the estimated activity distribution, and the process repeated until the agreement cannot be improved. Excellent image quality is possible, as this method can accurately model the statistical noise and camera response. The advantage of such algorithms is that they attempt to place activity only in the plane that the event originated in, and thus give a truer (and potentially quantitative) representation of the activity distribution. The main disadvantage is that they are computationally intensive and can take several hours to converge (depending on data set size).

We use Monte Carlo simulation to compare the images produced by the two geometries (planar and rectangular) and two reconstruction algorithm types (focal plane tomography and iterative) for a simple phantom. The iterative reconstruction algorithm used is the maximum likelihood algorithm followed by post-reconstruction spatial filtering [18]. The phantom simulated consists of a uniform activity concentration that fills the 7.5 cm x 7.5 cm x 10 cm field of view. In this volume there are seven spheres, each 8 mm in diameter and each filled with three times the activity concentration of the uniform background. One sphere is located at the center of the camera (0, 0, 0) and the other six are placed along the three axes half way between the camera center and the edge of the field of view (*i.e.* at (± 1.875 cm, 0, 0), at (0, ± 2.5 cm, 0), and at (0, 0, ± 1.875 cm)).

Images are reconstructed with the parallel plane camera using focal plane tomography, the parallel plane camera using iterative reconstruction, and the rectangular camera using iterative reconstruction. Attenuation is included in the simulation, but Compton scatter and random coincidences are not simulated. While the number of detected events is different for the rectangular and parallel plane geometries, both have the same number of annihilations generated; this number is chosen to yield the signal to noise ratio (when random and scattered events are included) that is expected for a 10 min. acquisition following a 1 mCi whole body injection into a 75 kg patient.

Figure 6 shows a horizontal (z=0) plane of each of the three 3-dimensional images reconstructed in these simulations. Figure 7 shows profiles along the x-axis of these three images; the x-axes would appear as vertical lines bisecting each of the images in Figure 6. Vertical (x=0) planes of the same three 3-dimensional data sets that produced Figure 6 are shown in Figure 8, and their profiles along the z-axis (which would appear as vertical lines bisecting the images in Figure 8) are shown in Figure 9. Both Figures 6 & 8 show that the reconstruction with the focal plane tomography has significantly less contrast than the two iterative reconstructions, as expected, and the focal plane reconstruction has some blurring in the z-direction in Figure 8 that is not observed with the iterative reconstruction. The profiles in Figures 7 & 9 show that there is indeed significantly less contrast (*i.e.*, peak to valley ratio) in the images obtained with focal plane tomography compared to the two iterative reconstructions.

The difference between the two iterative reconstructions is less significant. Figures 6 & 8 show slightly more background noise in the planar camera images than for the
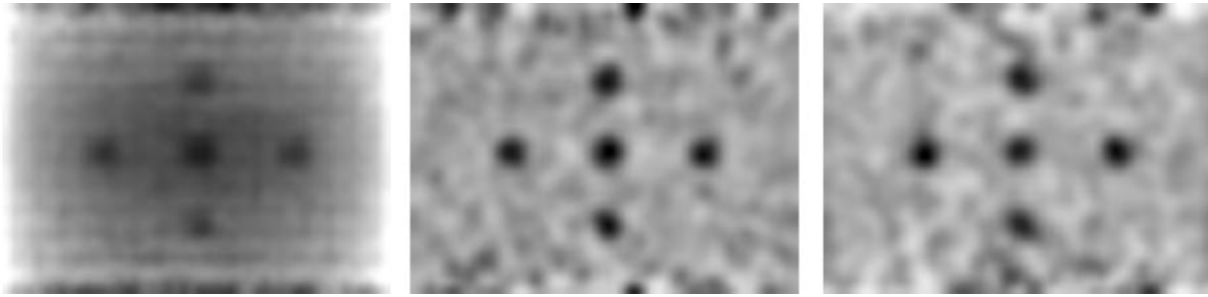
Figure 6. Reconstructed images of the central horizontal (z=0) plane of the field of view.
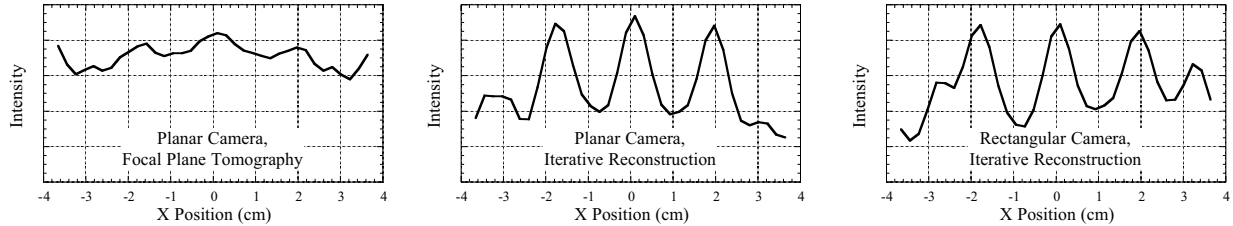
Figure 7. Projections through the middle of the three images in Figure 6. The correspond to projections along the x-axis.

rectangular camera images, and some "X" shaped diagonal streak artifacts (due to the incomplete angular coverage) are seen in the planar image in Figure 8. Little blurring along the z-axis is observed with either camera in Figure 8, as the mathematical model of the camera response accurately compensates for this the reduced angular coverage. It is possible that a different phantom geometry (with smaller diameter sources or sources placed near the edge of the field of view) would exacerbate this blurring.

VI. NON-INSTRUMENTATION ISSUES

Some of the limitations to PEM have nothing to do with camera design. For example, there is considerable interest in detecting small (3 mm diameter and below) tumors. However, small tumors will contain extremely low amounts of activity, and so may be very difficult to observe above the background activity level. Assuming a 10 mCi injection into a 75 kg patient and a 3:1 tumor to normal tissue uptake ratio (a typical value for fluoro-deoxyglucose, which is the most commonly used radiotracer for breast cancer), the expected activity concentration is 150 nCi/cc in normal tissue and 500 nCi/cc in tumors. This implies that during a 10 minute acquisition time there would be only 130,000 annihilations in a 3 mm diameter tumor, as compared to 5,000,000 annihilations in a 1 cm diameter tumor and 1.6 billion annihilations in the remainder of the 7.5 cm x 7.5 cm x 10 cm field of view. Thus, imaging small tumors will be difficult because the volume (and hence number of annihilations) scales as the cube of the tumor diameter.

In addition, there is significant patient to patient variation in the tumor activity concentration (or tumor to normal tissue ratio). The cause for this is not understood — a recent study searched for correlations between the tumor SUV (standard
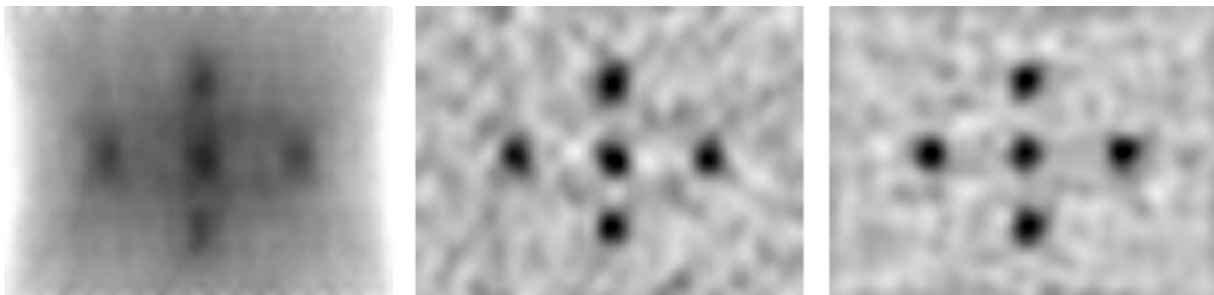
Figure 8. Reconstructed images of the central vertical (x=0) plane of the field of view.
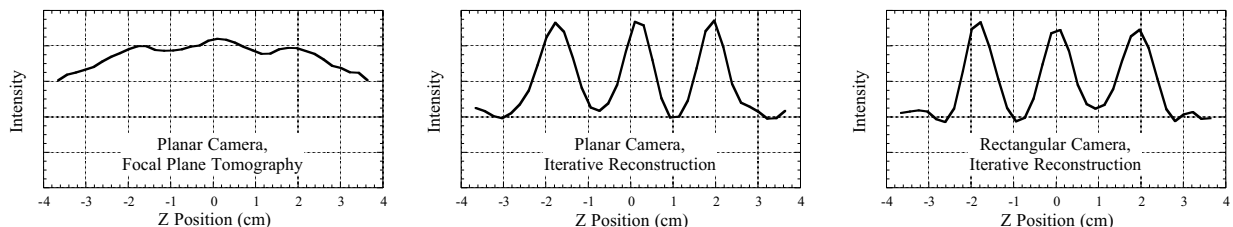
Figure 9. Projections through the middle of the three images in Figure 8. The correspond to projections along the z-axis.

uptake value, which is effectively a measure of the tumor to normal tissue ratio) for fluoro-deoxyglucose and over a dozen different histological and pathological measures of tumor characteristics (*e.g.*, size, grade, vascularity, estrogen and progesterone receptor status, mitotic figure, etc.) and either weak or no correlation was observed with each measure [19]. Thus, it is possible that an impeccably designed PEM camera will be unable to image a breast cancer tumor merely because the tumor, for unknown reasons, has a low radiotracer uptake.

VII. CONCLUSION

PEM offers significantly higher sensitivity for radiation sources in the breast than conventional PET cameras, mainly because of significantly increased solid angle coverage and reduced attenuation in the patient. The geometries employed require detector modules that are capable of measuring depth of interaction in order to minimize penetration artifacts and so simultaneously achieve high sensitivity and high spatial resolution. One would expect that different camera geometries (*e.g.* parallel plane or rectangular) and different reconstruction algorithms (*e.g.* focal plane tomography or iterative techniques) would significantly affect the imaging performance. In the simulations performed here, the reconstruction algorithm used had a major affect (the image quality of the iterative methods was significantly better than that with the focal plane tomography), while the different geometries (which have different solid angle coverage) had a lesser affect on the resulting image (although the rectangular geometry had less image noise). Finally, there are significant limitations due to non-instrumental effects, such as the absolute amount of radiotracer that is absorbed by the tumor.

VIII. ACKNOWLEDGMENT

IX. REFERENCES

[1] C. J. Thompson, K. Murthy, R. L. Clancy, et al., "Imaging performance of a PEM-I: A high resolution system for positron emission mammography," *IEEE Nucl Sci Symp and Med Imag Conf Rec*, vol. 2, pp. 1074-1078, 1995.

[2] W. W. Moses, T. F. Budinger, R. H. Huesman, et al., "PET camera designs for imaging breast cancer and axillary node involvement," *J. Nucl. Med.*, vol. 36, pp. 69P, 1995.

[3] I. Weinberg, S. Majewski, A. Weisenberger, et al., "Preliminary results for positron emission mammography

[4] R. Freifelder and J. S. Karp, "Dedicated PET scanners for breast imaging," *Physics in Medicine and Biology*, vol. 42, pp. 2463-2480, 1997.

[5] M. B. Williams, R. M. Sealock, S. Majewski, et al., "PET detector using waveshifting optical fibers and microchannel plate PMT with delay line readout," *IEEE Trans. Nucl. Sci.*, vol. 45, pp. 195–205, 1998.

[6] W. Worstell, O. Johnson, H. Kudrolli, et al., "First results with high-resolution PET detector modules using wavelength-shifting fibers," *IEEE Trans Nucl Sci*, vol. 45, pp. 2993-2999, 1998.

[7] N. K. Doshi, Y. P. Shao, R. W. Silverman, et al., "Design and evaluation of an LSO PET detector for breast cancer imaging," *Medical Physics*, vol. 27, pp. 1535-1543, 2000.

[8] K. Murthy, M. Aznar, A. M. Bergman, et al., "Positron emission mammographic instrument: Initial results," *Radiology*, vol. 215, pp. 280-285, 2000.

[9] R. R. Raylman, S. Majewski, R. Wojcik, et al., "The potential role of positron emission mammography for detection of breast cancer. A phantom study," *Medical Physics*, vol. 27, pp. 1943-1954, 2000.

[10] G. Muehllehner, "Resolution limit of positron cameras," *J. Nucl. Med.*, vol. 17, pp. 757–758, 1976.

[11] S. E. Derenzo, "Method for optimizing side shielding in positron emission tomographs and for comparing detector materials," *J. Nucl. Med.*, vol. 21, pp. 971-977, 1980.

[12] C. L. Melcher and J. S. Schweitzer, "Cerium-doped lutetium orthosilicate: a fast, efficient new scintillator," *IEEE Trans. Nucl. Sci.*, vol. NS-39, pp. 502–505, 1992.

[13] A. M. Cormack, "Representation of a function by its line integrals, with some radiological applications," *J. Appl. Phys.*, vol. 34, pp. 2722–2727, 1963.

[14] G. Muehllehner, M. P. Buchin, and J. H. Dudek, "Performance parameters of a positron imaging camera," *IEEE Trans. Nucl. Sci.*, vol. 23, pp. 528–537, 1976.

[15] C. J. Thompson, K. Murthy, Y. Picard, et al., "Positron Emission Mammography (PEM) - a promising technique for detecting breast cancer," *IEEE Trans. Nucl. Sci.*, vol. 42, pp. 1012-1017, 1995.

[16] N. J. Pelc, "A generalized filtered back-projection algorithm for three dimensional reconstruction," : Harvard School of Public Health, 1979.

[17] L. A. Shepp and Y. Vardi, "Maximum likelihood reconstruction for emission tomography," *IEEE Trans. Med. Img.*, vol. MI-1, pp. 113–122, 1982.

[18] R. H. Huesman, G. J. Klein, W. W. Moses, et al., "List-mode maximum-likelihood reconstruction applied to positron emission mammography (PEM) with irregular sampling," *IEEE Trans. Med. Imaging*, vol. 19, pp. 532–537, 2000.

[19] N. Avril, M. Menzel, J. Dose, et al., "Glucose metabolism of breast cancer assessed by F-18-FDG PET: Histologic and immunohistochemical tissue analysis," *J. Nucl. Med.*, vol. 42, pp. 9-16, 2001.

- real-time functional breast imaging in a conventional mammography gantry," *Euro. J. Nucl. Med.*, vol. 23, pp. 804-806, 1996.